SCIENTIFIC REPORTS

OPEN

Uncovering high-strain rate protection mechanism in nacre

Zaiwang Huang[1], Haoze Li[1], Zhiliang Pan[2], Qiuming Wei[2], Yuh J. Chao[1] & Xiaodong Li[1]

[1]Department of Mechanical Engineering, University of South Carolina, 300 Main Street, Columbia, South Carolina 29208, USA, [2]Department of Mechanical Engineering, University of North Carolina at Charlotte, 362, ERB, Charlotte, North Carolina 28223, USA.

SUBJECT AREAS:
MECHANICAL PROPERTIES
NANOPARTICLES
MATERIALS PHYSICS
APPLIED PHYSICS

Received
10 August 2011

Accepted
13 October 2011

Published
8 November 2011

Correspondence and requests for materials should be addressed to X.L. (lixiao@cec.sc.edu)

Under high-strain-rate compression (strain rate ~10^3 s^{-1}), nacre (mother-of-pearl) exhibits surprisingly high fracture strength vis-à-vis under quasi-static loading (strain rate 10^{-3} s^{-1}). Nevertheless, the underlying mechanism responsible for such sharply different behaviors in these two loading modes remains completely unknown. Here we report a new deformation mechanism, adopted by nacre, the best-ever natural armor material, to protect itself against predatory penetrating impacts. It involves the emission of partial dislocations and the onset of deformation twinning that operate in a well-concerted manner to contribute to the increased high-strain-rate fracture strength of nacre. Our findings unveil that Mother Nature delicately uses an ingenious strain-rate-dependent stiffening mechanism with a purpose to fight against foreign attacks. These findings should serve as critical design guidelines for developing engineered body armor materials.

Nacre (mother-of-pearl) has long been identified as the best natural armor material with superior mechanical strength and eminent fracture toughness[1-13]. Extensive work has thus far revealed that nacre is a hierarchically assembled nanocomposite, consisting primarily of highly organized polygonal aragonite (a polymorph of $CaCO_3$) platelets with thickness ranging from 200 to 500 nanometers and an edge length about 5 μm sandwiched with 5–20 nanometers thick organic biopolymer interlayers. Such an ingenious assembly strategy renders nacre a two fold increase in strength and some three orders of magnitude improvement in fracture toughness compared with aragonite, its primary constituent[1]. Several strengthening and/or toughening mechanisms, such as crack deflecting[4], interlocking[6,12], and mineral bridging[3,8], are believed to collectively contribute to nacre's mechanical robustness. However, nacre's basic building blocks, the individual aragonite platelets, have received less attention for their functional roles and working mechanisms in deformation and failure, in particular upon high-strain rate (dynamic) impact. Recent work showed that a single aragonite platelet with pseudo-single-crystal appearance is in fact composed of a number of nanoparticles with distinct individual orientations[14-17]. *In situ* atomic force microscopy revealed that the individual aragonite platelets are not brittle, but instead ductile owing to the nanoparticle rotation and deformation[17]. In fact, in view of nacre's real living environment, several key questions are raised, yet await answers: how does nacre protect itself from a high-speed predatory penetrating attack[5,13]? Does nacre trigger new mechanisms in response to high-strain-rate, ballistic impact or dynamic loading? If yes, are such mechanisms different from those operating in quasi-static mode? To address these critical questions, we are in a pressing need for an in-depth understanding of the structure-property relationship of nacre under both quasi-static and high-strain rate loading conditions. In this context, here we have designed a group of uniaxial compression experiments at both quasi-static and dynamic loading rates. We used the well-articulated Split-Hopkinson Pressure Bar (SHPB) system to perform high strain rate (~10^3 s^{-1}) compression to simulate the real predatory penetrating impacts (typically 10^2~10^3 s^{-1})[18] that nacre typically undergoes in the sea. We found that nacre exhibits superior damage tolerance and much elevated fracture strength upon dynamic loading. Based on detailed electron microscopic analysis, we attribute such phenomena to the emission of partial dislocations and the onset of deformation twinning within the nanometer-sized particles. The occurrence of these two types of defects is in keeping with the strikingly high strain rate sensitivity and the corresponding very small activation volumes associated with the plastic deformation of nacre, as derived from the experimental data.

Results

Figure 1 plots the true stress-true strain curves to demonstrate the quasi-static and dynamic compression behavior of nacre along its transverse direction. It should first be pointed out that global plastic deformation

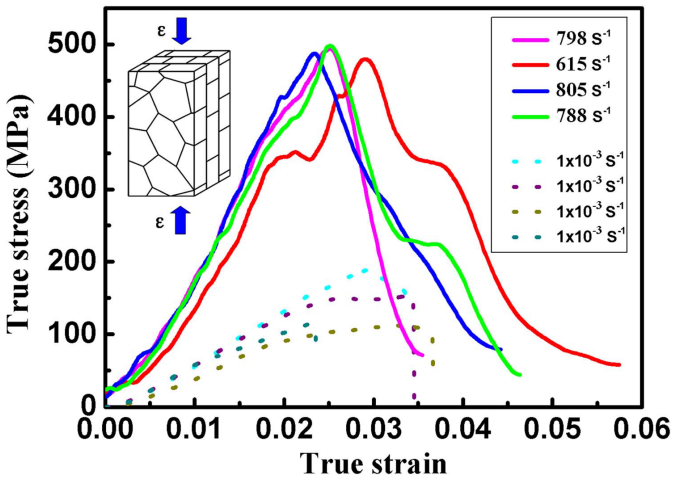

Figure 1 | Mechanical behavior of nacre under quasi-static (10^{-3} s^{-1}) and dynamic (~10^{3} s^{-1}) compression. The stress-strain curves show that maximal compressive stresses in dynamic compression are typically as high as 500 MPa, far exceeding those (generally below 200 MPa) in quasi-static mode, whereas the plastic strain amounts do not sacrifice (2%~4%) sharply.

of nacre under either condition is very limited. Under quasi-static loading (the dotted curves) the fracture strength shows quite scattered results, ranging within 80–200 MPa, the corresponding total plastic strains are generally lower than 4%, in good agreement with previous results[5]. In sharp contrast to this is the dynamic fracture strength values (the peak stresses in the solid lines), which are typically in the range of 450–500 MPa. Such are statistically 2~3 times higher than those measured in the quasi-static compression. The large discrepancy of fracture strength values between quasi-static and dynamic loading suggests a strong strain rate dependence of nacre's mechanical properties (Section 1 in supplementary materials). A quantitative evaluation based on the experimental results yields a strain rate sensitivity in the order of 0.09~0.18 (Section 2 in supplementary materials). Considering that almost all ceramic materials are rate-insensitive, or even exhibit negative rate-dependence, this finding with nacre is significant and needs further elaboration. The strong rate dependence of nacre is particularly relevant in the context of its use as body armor against external dynamic impact. With good reasons we can dub this behavior "dynamic self-stiffening".

We then encounter an immediate question: what physical mechanisms render nacre such remarkable "dynamic self-stiffening" properties? Or what functional roles does nacre evoke behind the physical mechanisms? Direct high resolution transmission electron microscopy (HRTEM) inspections on post-mortem samples will be presented to elucidate the aforementioned question. The HRTEM image of Figure 2a indicates that, upon quasi-static loading, the aragonite platelets consist of irregular-shaped nanoparticles with random crystallographic orientations. The blow-up of the boxed area of Figure 2a shows that at least four nanoparticles with an average particle size of a few nanometers are incorporated. No preferential crystallographic orientations can be associated with these nanoparticles (Figure 2b). This indicates that the previously inter-parallel crystallographic orientations with a pseudo-single-crystal characteristic in the pristine aragonite platelets[15] have given way to random orientation due to the nanoparticle rotation and deformation during the quasi-static loading process. This is further confirmed by the messy, though spot-like electron diffraction pattern (Figure 2c). We thus suggest that such small particle size (a few nanometers) can effectively restrain full dislocation activities, and the particle boundary-mediated processes may have taken a leading role in the crystal plasticity of nacre. A similar working mechanism has been reported in a nanocrystalline Ni film[20].

In contrast, upon high-strain-rate loading, a distinct change in deformation mechanism was detected within individual aragonite platelets. Figure 3a depicts a representative TEM image showing high density of nanoparticles randomly packed together, featured by a ring-like electron diffraction pattern (the inset). Careful measurements on the HRTEM lattice image show that the nanoparticle sizes are of the same order of magnitude as those upon quasi-static loading. However, a closer-up examination based on atom-to-atom measurement and analysis (Figure 3b) on the white-boxed area indicates that lattice irregularities have been triggered in individual particles. This can be identified as the consequence of partial dislocation activities, a new crystallographic defect never reported in pristine nacre to the best of our knowledge. The atomic details indicate that the regular sequence of atomic stacking terminates at the positions marked by the red arrows in Figure 3b and the atoms (white arrowed) slide to another crystallographic plane by introducing a Burgers vector $\vec{b}_1$.

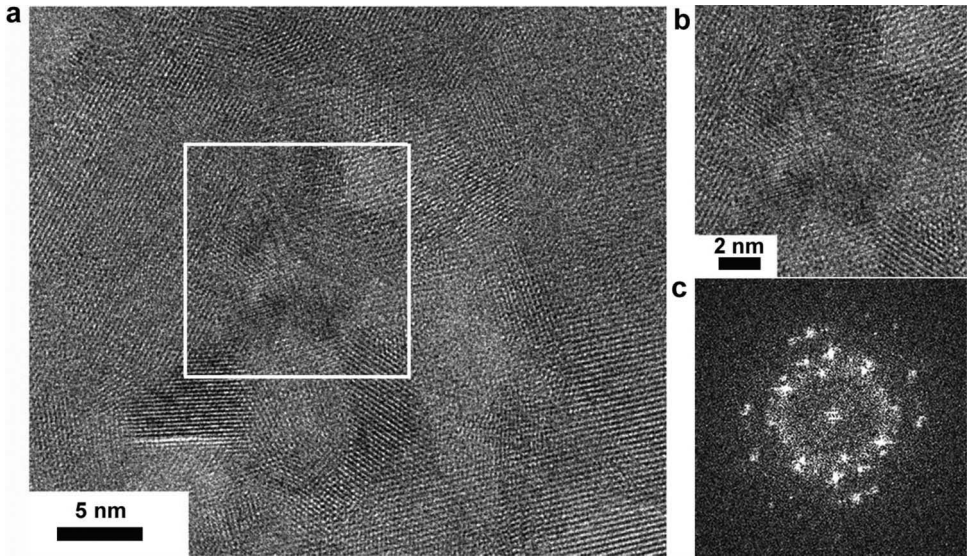

Figure 2 | Disordered aragonite nanoparticles in quasi-statically deformed nacre. (a) When deformed, aragonite nanoparticles are rearranged in a disorganized manner. (b) a closer-up view of the white boxed area shows that at least four nanoparticles with random orientations piled up in this area. (c) From the corresponding area (b) the FFT scatters a messy-spot diffraction pattern.

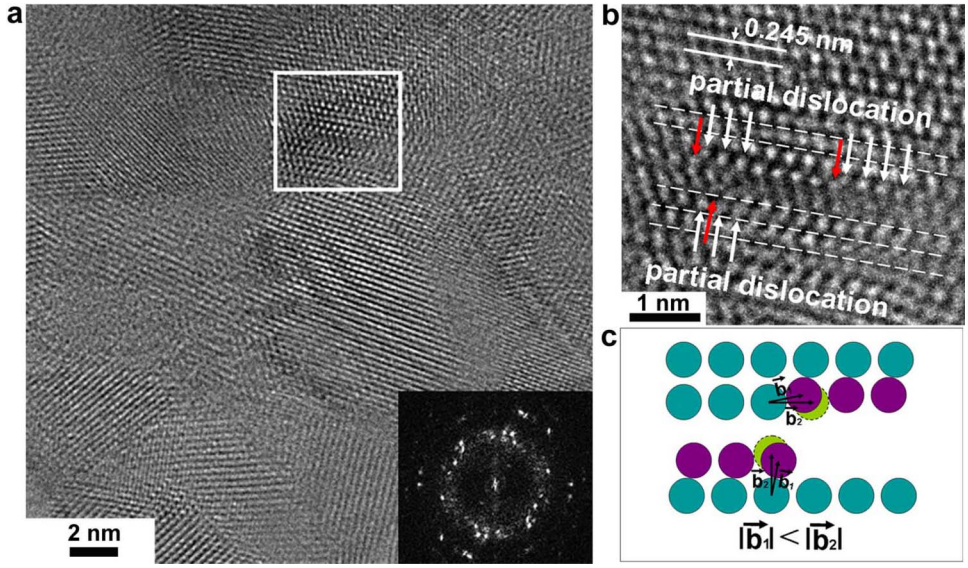

Figure 3 | Analysis of partial dislocations in dynamically deformed nacre. (a) The region with disordered nanoparticles scatters ring-like diffraction pattern (inset), indicating that a process involving particle boundary-mediated deformation has taken place. (b) In detail, new crystallographic irregularity within one particle (white boxed) can be measured and analyzed with a point-to-point resolution. (c) a partial dislocation can be determined by the characterization and measurement of burgers vector, which is schematically illustrated.

This is better visualized as a partial dislocation by $\left|\vec{b}_1\right| < \left|\vec{b}_2\right|$ along a specific crystallographic orientation. Figure 3c is a schematic illustration demonstrating how the partial dislocation is recognized via measuring the atomic spacing, where $\vec{b}_2$ represents a unit cell vector in aragonite, the magnitude of which equals an integer multiples of the atomic spacing. In this regime, absence of full dislocation nucleation can be attributed to the geometrically-limited particle size, therefore leading to the nucleation and propagation of partial dislocations from the particle boundaries. Such transgranular-like process under dynamic loading is believed to contribute to the increase of nacre's strength compared to intergranular-like deformation behavior under quasi-static loading[21].

It has been well documented that both microstructure alteration[22,23] and external factor optimization[24-26] can trigger deformation twinning, which is not prevalent in most conventional crystalline solids. HRTEM image (Figure 4a), however, reveals that nanoscale deformation twinning can be set into play in the orthorhombic aragonite crystals upon dynamic loading. Such deformation twinning (Figure 4b) can be identified by appearance of the mirror symmetry between the matrix and the twin band, ubiquitous in the atomic resolution image and the corresponding Fast Fourier Transform (FFT) (the inset) showing a dual-spot diffraction characteristic of twinning. A closer-up view of the matrix-twin interface (white box enclosed) reveals that the twin boundary (TB) is atomically sharp, but not perfectly coherent. The twin plane can be indexed as the (110) plane (Figure 4b). Through coupling the lattice image and the corresponding FFT pattern (Figure 4c), the symmetric crystal plane is determined to be the (1 1 0) plane with an inclination angle

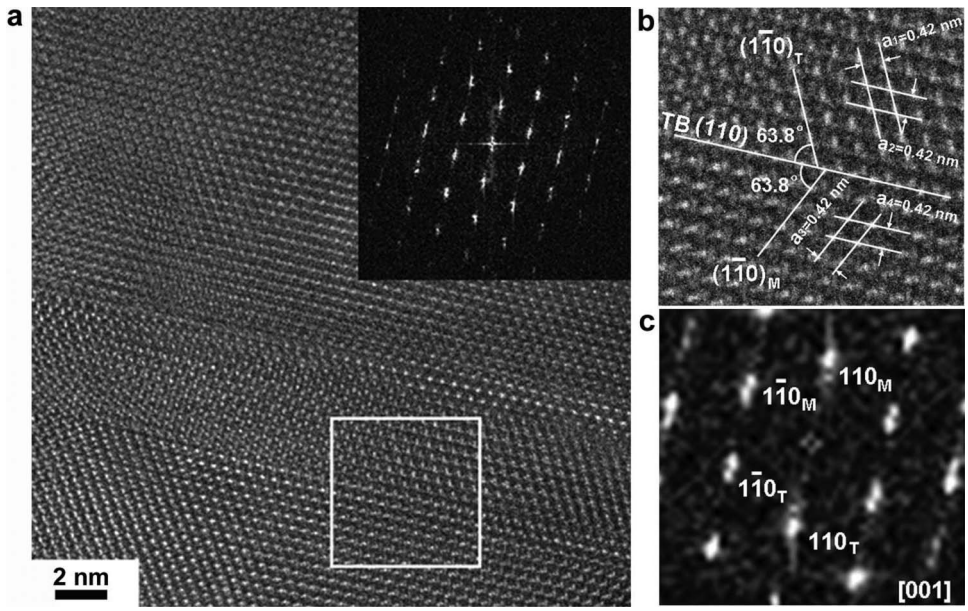

Figure 4 | TEM observation of deformation twinning in dynamically deformed nacre. (a) HRTEM image of deformation twinning. The inset is the confirmation of twinning using FFT analysis. (b) A closer-up view of the twinning boundary and its mirror symmetry relationship from white boxed area. (c) The FFT showing the twinning relationship between narrow band and matrix.

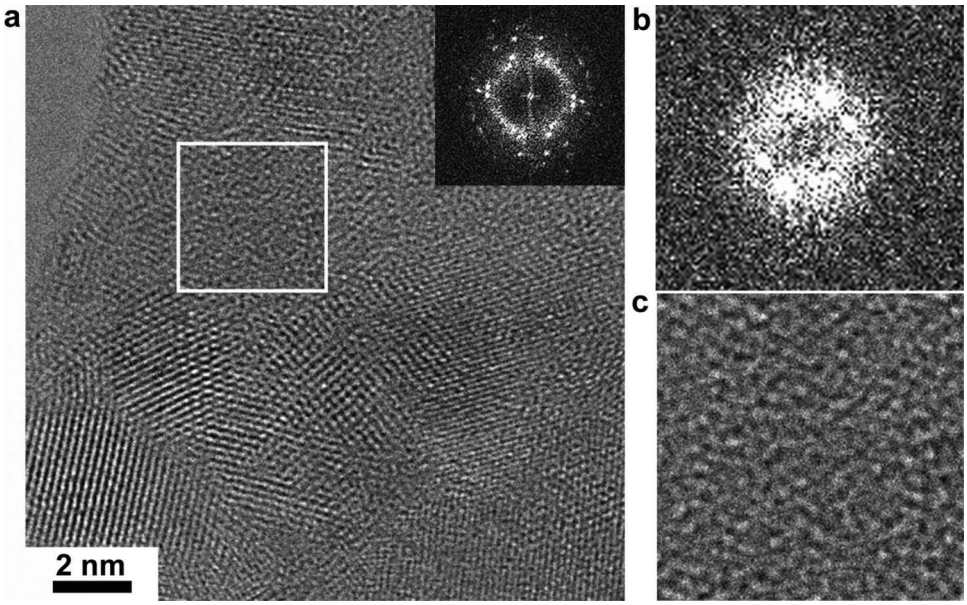

Figure 5 | Amorphous aggregation in dynamically deformed nacre. (a) Amorphous aggregation is surrounded by aragonite nanoparticles with random orientations characterized by FFT pattern (inset). (b) FFT without clear spot pattern from white boxed region shows a characteristic of amorphous aggregation. (c) A closer-up view of amorphous aggregation from corresponding white boxed area in (a) shows a mosaic feature.

of 63.8° to the TB plane. Measurements demonstrate that the twin lamella is a few nanometers wide, and it approximately equals ten (110) plane spacing between two parallel planar faults. The occurrence of deformation twinning is generally accompanied with partial dislocation nucleation and emission from grain boundaries. A similar example in aluminum[24] has uncovered the evolution details through computer simulation, where the deformation twinning is generated by the successive emission of partial dislocations from the same grain boundary on neighboring (111) planes. In this regard, the leading partial nucleates and glides through the whole grain and leaves in its wake a stacking fault, and subsequently a twinning partial with the same Burgers vector ensues. This operation eventually evolves into a deformation twin that has been confirmed by experimental observations[22,23].

Discussion

Quantitatively, the activation volume (v*) of plastic deformation, delineating the physical domain of plastic deformation events, can be linked to the strain rate sensitivity (SRS)[27] as

$$v^* = \frac{\sqrt{3}\cdot k\cdot T}{\sigma\cdot m} \qquad (1)$$

Here k is the Boltzmann constant (1.38×10^{-23} m^2 kg $s^{-2}k^{-1}$), T is absolute temperature, and σ and m are respectively the effective stress and the SRS. Clearly the activation volume can be used as a finger-print of the deformation mechanisms. Based on the experimental results of this work, the SRS of nacre is in the order of ~0.1, which in turn corresponds to an activation volume in the order of a few b^3 (Section 2 in supplementary materials). This implies that local plastic deformation is readily activated upon dynamic loading, even though the plasticity may not be sustainable as evidenced from the lack of global plastic deformation of the dynamic specimens. As a result, relatively "harder" physical mechanisms, i.e., partial dislocation emission and deformation twinning (see more deformation twinning in section 3 of supplementary materials), debut as increasing applied stress induced by enhancing strain rate. In contrast, comparatively "easier" dislocation mechanisms, such as dislocation slip and grain boundary rearrangement, are prevalent owing to large activation volumes at lower loading rates[27]. We believe that the emerging partial dislocations and deformation twinning in nacre are strongly correlative with the miniaturized activation volume. Finally, a significant fact should be noted that on the basis of our evaluation (Section 4 in supplementary materials) individual aragonite platelets act as dominating "carriers" in overall strength enhancement, whereas the contribution of biopolymer to rate-strengthening remains quite limited due to its low volume fraction (5 vol. %) as well as its low mechanical stiffness.

In orthorhombic aragonite, the atomic configuration and crystal structure are far more complicated than those more common FCC/BCC metals. We suggest that dynamic loading and the extremely small dimensions of the aragonite nanoparticles work together to restrain full dislocation-related activities. As a consequence, nacre appeals to the alternative harder mechanisms such as partial dislocations and deformation twinning, explaining its dynamic self-stiffening behavior. These findings significantly advance our understanding of nacre's design principles and provide guidelines for optimizing the damage tolerance design of engineered nacre-inspired materials. We have to note, though, that the formation and evolution mechanisms of partial dislocations and deformation twinning in orthorhombic aragonite still remain an open question to be explored. Atomistic simulation and modeling may help to shed light into this arena.

Another question that may follow is: What are the structural details at the nanoparticle boundary/interface in nacre after dynamic loading? Our previous TEM results[15] showed that at least two types of imperfect transition exist in pristine nacre: screw dislocation and amorphous aggregation. A large number of dislocation events from particle boundary/interface are believed to result in an irregular and complex atomic configuration. Figure 5a demonstrates an amorphous aggregation regime encircled (white boxed area) by nanoparticles after dynamic compression, where the messy spot diffraction pattern (inset) indicates that previously ordered arrangements of aragonite nanoparticles in pristine nacre have been completely destroyed. The amorphous phase is further confirmed by FFT (Figure 5b) that scatters into a halo feature. An extremely important detail is that the amorphous zone extends to at least four nanometers in size (Figure 5c), which was not observed in the fresh and the quasi-statically deformed nacre samples. The direct response is the elongation of the pre-existing amorphous particle boundary (two nanometers in size at most, based on our observation). However, although no direct evidence is at hand, we suggest that the metastable

aragonite crystalline phase has probably in part transformed to an amorphous phase, which is extensively found in the dynamically compressed nacre samples along c-axis. A similar case was reported by Chen and co-workers in ballistically tested boron carbide[28]. We expect that such phase transformation may improve nacre's high-strain rate performance. In addition, our observation conversely confirms the previous conclusion[15] that amorphous aggregation is an important transition phase acting as "grain boundaries" between the nanoparticles.

In summary, we demonstrate for the first time solid evidence that two new deformation mechanisms, partial dislocation emission and deformation twinning, are triggered in nacre's aragonite platelets under high-strain-rate uniaxial compression, which renders a much elevated fracture strength in comparison to quasi-static loading. This dynamic self-stiffening behavior benefits nacre's self-protection from predatory penetrating attack. These findings advance our understanding of damage tolerance design principle in engineered body armor materials.

Methods

In this Report, natural nacre materials from California red abalone (Haliotis rufescens) that belong to the class of gastropoda were chosen for the investigation. The shells were collected alive in Santa Barbara, CA. To minimize the detrimental effect of drying on the structure and mechanical behavior of the shells, they were cleaned and then air delivered in ice to the laboratory where the experiments were conducted. The nacre samples were cut from the nacrous layer of the shells with a water-cooled, low-speed diamond saw. Then the nacre samples were rinsed thoroughly with distilled water. The quasi-static and dynamic uniaxial compression tests were respectively carried out with an Instron 5566 universal testing machine and a SHPB system[19]. Upon dynamic loading, the samples were pulverized. The post-mortem powders were immediately collected and dispersed in distilled water with ultrasonic wave for two hours. The powders were then transferred onto the holey carbon-coated copper film for analysis with a JEOL JEM 2100F high resolution transmission electron microscope (HRTEM) at an accelerating voltage of 200 KV.

1. Currey, J. D. Mechanical properties of Mother of Pearl in tension. *Proc. R. Soc. London Ser. B* **196**, 443–463 (1977).
2. Jackson, A. P., Vincent, J. F. V.& Turner, R. M. The mechanical design of nacre. *Proc. R. Soc. London Ser. B* **234**, 415–440 (1988).
3. Schaffer, T. E. *et al.* Does abalone nacre form by heteroepitaxial nucleation or by growth through mineral bridges? *Chem. Mater.* **9**, 1731–1740 (1997).
4. Feng, Q. L. *et al.* Crystal orientation, toughening mechanism and a mimic of nacre. *Mater. Sci. Eng. C* **11**, 19–25 (2000).
5. Menig, R., Meyers, M. H., Meyers, M. A. & Vecchio, K. S. Quasi-static and dynamic mechanical response of *Haliotis Rufescens* (Abalone) shells. *Acta Mater.* **48**, 2383–2398 (2000).
6. Wang, R. Z. *et al.* Deformation mechanisms in nacre. *J. Mater. Res.* **16**, 2485–2493 (2001).
7. Gao, H. J. *et al.* Materials become insensitive to flaws at nanoscale: lessons from nature. *Proc. Natl. Sci. U.S.A.* **100**, 5597–5600 (2003).
8. Song, F., Soh, A. K. & Bai, Y. L. Structural and mechanical properties of the organic matrix layers of nacre. *Biomaterials* **24**, 3623–3631 (2003).
9. Nassif, N. *et al.* Amorphous layer around aragonite platelets in nacre. *Proc. Natl. Acad. Sci. U.S.A.* **102**, 12653–12655 (2005).
10. Rousseaua, M. *et al.* Multiscale structure of sheet nacre. *Biomaterials* **26**, 6254–6262 (2005).
11. Barthelat, F., Li, C. M., Comi, C. & Espinosa, H. D. Mechanical properties of nacre constituents and their impact on mechanical performance. *J. Mater. Res.* **21**, 1977–1986 (2006).
12. Katti, S. K., Mohanty, B. & Katti, D. R. Nanomechanical properties of nacre. *J. Mater. Res.* **21**, 1237–1242 (2006).
13. Ortiz, C. & Boyce, M. C. Bioinspired structural materials. *Science* **319**, 1053–1054 (2008).
14. Li, X. D. *et al.* Nanoscale structural and mechanical characterization of a natural nanocomposite material: The shell of red abalone. *Nano Lett.* **4**, 613–617 (2004).
15. Li, X. D. & Huang, Z. W. Unveiling the formation mechanism of Pseudo-single-crystal aragonite platelets in nacre. *Phys. Rev. Lett.* **102**, 075502 (2009).
16. Huang, Z. W. & Li, X. D. Nanoscale structural and mechanical characterization of heat treated nacre. *Mater. Sci. Eng. C* **29**, 1803–1807 (2009).
17. Li, X. D., Xu, Z. H. & Wang, R. Z. In situ observation of nanograin rotation and deformation in nacre. *Nano Lett.* **6**, 2301–2304 (2006).
18. Nietzel, D. A. *et al. Laboratory research.* (2000).
19. Wei, Q. *et al.* Mechanical behavior and dynamic failure of high-strength ultrafine grained tungsten under uniaxial compression. *Acta Mater.* **54**, 77–87 (2006).
20. Shan, Z. W. *et al.* Grain boundary-mediated plasticity in nanocrystalline nickel. *Science* **305**, 654–657 (2004).
21. Chen, M. W., McCauley, J. W., Dandekar, D. P. & Bourne, N. K. Dynamic plasticity and failure of high-quality alumina under shock loading. *Nat. Mater.* **5**, 614–618 (2006).
22. Chen, M. W. *et al.* Deformation twinning in nanocrystalline aluminum. *Science* **300**, 1275–1277 (2003).
23. Liao, X. Z. *et al.* Deformation mechanism in nanocrystalline Al: Partial dislocation slip. *Appl. Phys. Lett.* **83**, 632–634 (2003).
24. Yamakov, V. *et al.* Dislocation processes in the deformation of nanocrystalline aluminium by molecular-dynamics simulation. *Nat. Mater.* **1**, 45–48 (2002).
25. Warner, D. H., Curtin, W. A. & Qu, S. Rate dependence of crack-tip processes predicts twinning trends in f.c.c metals. *Nat. Mater.* **6**, 876–881 (2007).
26. Bringa, E. M. *et al.* Ultrahigh strength in nanocrystalline materials under shock loading. *Science* **309**, 1838–1841 (2005).
27. Wei, Q. Strain rate effects in the ultrafine grain and nanocrystalline regimes-influence on some constitutive responses. *J. Mater. Sci.* **42**, 1709–1727 (2007).
28. Chen, M. W., McCauley, J. W. & Hemker, K. J. Shock-induced localized amorphization in boron carbide. *Science* **299**, 1563–1566 (2003).

Acknowledgements

We thank R. Z. Wang for providing the nacre samples. This work was supported by the U. S. Army Research Office under agreement/grant No. W911 NF-07-1-0449. Q. M. Wei was grateful for the financial support of U.S. Army Research Office under Grant No. W911NF-07-1-0335.

Author contributions

Z. H. and X. L. designed the project, Z. H., H.L. and Z.P. carried out the experiments, Z. H., Q. W. and X. L. wrote this paper, all the authors contributed to the discussion.

Additional information

Supplementary information accompanies this paper at http://www.nature.com/scientificreports

Competing financial interests: The authors declare no competing financial interests.

How to cite this article: Huang, Z. *et al.* Uncovering high-strain rate protection mechanism in nacre. *Sci. Rep.* **1**, 148; DOI:10.1038/srep00148 (2011).